ChemPubSoc Europe

DOI: 10.1002/cssc.201600776

CHEMSUSCHEM Full Papers

Selectivity Control in the Tandem Aromatization of Bio-Based Furanics Catalyzed by Solid Acids and Palladium

Homer C. Genuino,[a] Shanmugam Thiyagarajan,[a, b] Jan C. van der Waal,[c] Ed de Jong,*[c] Jacco van Haveren,[b] Daan S. van Es,*[b] Bert M. Weckhuysen,[a] and Pieter C. A. Bruijnincx*[a]

Bio-based furanics can be aromatized efficiently by sequential Diels–Alder (DA) addition and hydrogenation steps followed by tandem catalytic aromatization. With a combination of zeolite H-Y and Pd/C, the hydrogenated DA adduct of 2-methylfuran and maleic anhydride can thus be aromatized in the liquid phase and, to a certain extent, decarboxylated to give high yields of the aromatic products 3-methylphthalic anhydride and *o*- and *m*-toluic acid. Here, it is shown that a variation in the acidity and textural properties of the solid acid as well as bifunctionality offers a handle on selectivity toward aromatic products. The zeolite component was found to dominate selectivity. Indeed, a linear correlation is found between 3-methylphthalic anhydride yield and the product of (strong acid/total acidity) and mesopore volume of H-Y, highlighting the need for balanced catalyst acidity and porosity. The efficient coupling of the dehydration and dehydrogenation steps by varying the zeolite-to-Pd/C ratio allowed the competitive decarboxylation reaction to be effectively suppressed, which led to an improved 3-methylphthalic anhydride/total aromatics selectivity ratio of 80% (89% total aromatics yield). The incorporation of Pd nanoparticles in close proximity to the acid sites in bifunctional Pd/H-Y catalysts also afforded a flexible means to control aromatic products selectivity, as further demonstrated in the aromatization of hydrogenated DA adducts from other diene/dienophile combinations.

Introduction

The high volatility of crude oil markets as well as the implementation of shale gas as a new hydrocarbon resource can strongly impact the availability of some important commodity chemicals, including bulk aromatics.[1] Sugar-derived furanics offer an alternative sustainable resource for the production of "drop-in" renewable aromatics that include terephthalic, (iso)-phthalic, and trimellitic aromatic acids, which are essential precursors to various polymer products and fine chemicals.[2]

Furanics-to-aromatics routes generally involve a two-step catalytic conversion that consists of a symmetry-allowed [4+2] Diels–Alder (DA) cycloaddition of a furanic diene with an appropriate dienophile followed by a catalytic aromatization step. An example of this route is the production of *p*-xylene from ethylene and bio-based 2,5-dimethylfuran (DMF) by solid-acid-catalyzed DA aromatization. For example, Williams et al. used zeolite H-Y with a Si/Al ratio of 30 and zeolite H-Beta with a Si/Al ratio of 12.5 for this reaction in heptane to achieve 75 and 90% *p*-xylene yields, respectively.[3] Wang et al. later demonstrated the synthesis of renewable benzene, toluene, and *p*-xylene from (methylated) furans, also with ethylene, using various heterogeneous catalysts.[4] Brønsted acid and Lewis acid containing catalysts, such as WO_x-ZrO_2, niobic acid, zeolite H-Y, and silica-alumina, were more active than catalysts that contained predominantly Lewis acid sites, such as γ-Al_2O_3 and TiO_2 (P25), which emphasizes the importance of strong Brønsted acidity in the production of aromatics.[4] In contrast, Davis et al. showed that silica molecular sieves that contained framework Lewis acid centers (e.g., Sn-, Zr-, and Zn-β zeolites), catalyze the DA cycloaddition–dehydration reactions between oxidized derivatives of 5-hydroxymethylfurfural (HMF) and ethylene more efficiently than the corresponding Brønsted acidic H-Al-β zeolite to give renewable-based terephthalic acid precursors.[5]

[a] Dr. H. C. Genuino, Dr. S. Thiyagarajan, Prof. Dr. B. M. Weckhuysen, Dr. P. C. A. Bruijnincx
Inorganic Chemistry and Catalysis
Debye Institute for Nanomaterials Science
Utrecht University
Universiteitsweg 99, 3584 CG Utrecht (The Netherlands)
E-mail: p.c.a.bruijnincx@uu.nl

[b] Dr. S. Thiyagarajan, Dr. J. van Haveren, Dr. D. S. van Es
Food & Bio-based Research
Wageningen University and Research Centre
P.O. Box 17, 6700 AA Wageningen (The Netherlands)
E-mail: daan.vanes@wur.nl

[c] Dr. J. C. van der Waal, Dr. E. de Jong
Avantium Chemicals
Zekeringstraat 29, 1014 BV Amsterdam (The Netherlands)
E-mail: ed.dejong@avantium.com

Supporting information and the ORCID identification number(s) for the author(s) of this article can be found under http://dx.doi.org/10.1002/cssc.201600776.

This publication is part of a Special Issue celebrating "10 years of ChemSusChem". To view the complete issue, visit: http://dx.doi.org/10.1002/cssc.v10.1.

An important general limitation of the coupling of the key DA reaction directly with the catalytic aromatization step is the thermal instability of the intermediate DA adduct, which is the result of the reversible nature of the DA reaction.[6] Therefore, catalytic DA aromatization reactions need to be performed typically either at a low temperature or a high ethylene pressure to limit retro-DA activity. Addressing this competition between aromatization by acid-catalyzed dehydration and the loss of the DA adduct to retro-DA, Mahmoud et al. reported a two-step route to (substituted) phthalic anhydrides by separating the DA addition step from dehydration and using methanesulfonic acid with acetic anhydride for the latter step.[6a] In an alternative approach, we recently developed a three-step, furanics-to-aromatics route by introducing an intermediate, mild hydrogenation step after the DA addition of, for example, 2-methylfuran (MF) and maleic anhydride (MA). The thermally stable oxanorbornane adduct (denoted as MFMA[H]) was then obtained in a high yield and purity.[7] The subsequent one-pot, tandem catalytic dehydration and dehydrogenation of the hydrogenated DA adduct in toluene then allowed efficient aromatization to yield the desired aromatic product, in this case 3-methylphthalic anhydride, with some concomitant formation of *o*- and *m*-toluic acid as decarboxylated products.[7] A γ-lactone, formed by the acid-catalyzed isomerization of MFMA[H], was identified as the primary intermediate in the aromatization reaction. The use of a physical mixture of Very Ultra Stable H-Y zeolite (H-VUSY) with a Si/Al ratio of 6 as a solid Brønsted acid and Pd/C as a dehydrogenation catalyst thus allowed the efficient aromatization of MFMA[H] by this new liquid-phase route to give high total aromatics yields.[7]

We also showed recently that the hydrogenated DA adducts can be converted conveniently to renewable aromatics in a solid-phase reaction using only a solid acid, that is, zeolite H-Y with a Si/Al ratio of 2.6, as the catalyst without any solvent or dehydrogenation catalyst, to give the same aromatic products in high yield.[8] Notably, for both the liquid- and solid-phase aromatization processes, some variation in the solid acid catalyst used already suggested that the selectivity to the desired aromatics depends strongly on the structural characteristics of the solid acid catalyst, in particular, its acidity and micro/mesoporosity.

Among the different solid acids tested, the large-pore zeolite H-Y with FAU topology performed the best in the aromatization reaction.[7,8] The retention of molecules within the zeolite crystal as a result of slow mass transfer through the micropores can potentially lead to catalyst deactivation by carbonaceous material deposition.[9] To ensure optimal active site accessibility and to enhance the molecular transport of reactants and products, mesopores in zeolite H-Y are commonly introduced by postsynthetic modifications, such as sequential steam–calcination and acid leaching, which result in an increased external surface area and pore volume.[9,10] Hierarchical FAU-type zeolites are thus formed with enhanced hydrothermal stability and altered compositions (i.e., Si/Al ratio) caused by the removal of part of the framework Al from the lattice to form extra-framework Al (EFAl) species, accompanied by changes in intrinsic acidity.[10]

The influence of the acidity of solid catalysts has been studied in some detail in the direct DA aromatization of DMF and ethylene. Williams et al. showed that good selectivity to *p*-xylene can be achieved at both low and high DMF conversion with an H-Y-2.6 zeolite as the catalyst.[3a] Interestingly, H-Y zeolites with Si/Al ratios of 2.6, 30, and 40 showed almost identical catalytic performances, and the *p*-xylene production rates were independent of the number of available Brønsted acid sites (BAS), which suggests a noncatalytic rate-limiting step.[3a] In a separate study in which WO_x-ZrO_2 was used as the catalyst, Wang et al. showed that the *p*-xylene production rate was linearly dependent on the amount of acid sites instead.[4] Theoretical studies by Patet et al. later proposed this difference to be result of a kinetic regime change in this tandem reaction and to be typical for coupled uncatalyzed–catalyzed steps.[11]

In our previous study, involving a reaction that must be mechanistically different from the above-mentioned studies, we observed that H-VUSY (H-Y with a Si/Al ratio of 6) produces a higher total aromatics yield (84%) than steam-calcined-only H-Y with a Si/Al ratio of 2.6 (75%) at full conversion,[7] which shows that performance in this case is not simply dictated by the number of acid sites. It can thus be anticipated that the type, amount, and strength of the acid sites and any mesoporosity in H-Y zeolites will play important roles in the overall catalyst efficiency for this aromatization reaction.[10e] Variation of mesoporosity can, for example, limit side reactions and prevent carbon loss. Therefore, the careful tuning of both acidity and porosity of zeolite H-Y-based catalysts is expected to allow control over selectivity to the desired aromatic product. As the reaction to and the first step from the γ-lactone intermediate are purely acid catalyzed,[8] we here first explore the interplay between the acidity and porosity of various zeolite H-Y materials to control aromatic product selectivity in the liquid-phase reaction in the absence of a separate dehydrogenation catalyst. Given that the presence of a dehydrogenation catalyst improves the total aromatics yield significantly,[7] the ratio of Pd (e.g., Pd/C) to H-Y in the physical mixture was also varied with the goal to further increase the yield and selectivity to the desired aromatic product. Finally, as the solid-acid- and Pd-catalyzed steps in the tandem reaction are coupled,[7] bifunctional catalysts with Pd in close proximity to the acid functionalities were expected to improve catalyst performance and have been evaluated.

Results and Discussion

Catalyst characterization

Four different H-Y zeolites with Si/Al molar ratios that ranged from 2.6 to 40 were studied in the aromatization of the MFMA[H] adduct. These materials are denoted as H-Y-*x* in which *x* is the Si/Al ratio of the material. Zeolite H-Y-2.6 was steamed by the manufacturer, NH_4-Y (Si/Al = 2.55) being the parent zeolite.[10c,12] Ultrastable Y zeolites are typically prepared by steaming of NH_4-Y-2.55 at ~500 °C, a second steaming step at ~700 °C, and finally acid-leaching to obtain the desired Si/Al ratio.[10c,12] For example, H-Y-6 was steamed and acid-leached

Table 1. Textural and acidic properties of fresh and reused solid acid catalysts, including the Pd-loaded catalyst materials.[a]

Solid acid catalyst	BET surface area [$m^2 g^{-1}$]	*t*-plot external surface area [$m^2 g^{-1}$]	*t*-plot micropore area [$m^2 g^{-1}$]	*t*-plot micropore volume [$cm^3 g^{-1}$]	Mesopore volume [$cm^3 g^{-1}$]	Total pore volume [$cm^3 g^{-1}$]	BJH average pore diameter [nm]	Amount, type, and strength of acid sites [($mmol_{NH_3}$ g^{-1} STP) (T_{max} [°C]) weak	strong
H-Y-2.55[b]	529	19	511	0.20	0	0.20	1.21	1.09 (225)	
H-Y-2.6	556	83	473	0.23	0.16	0.39	4.1	0.33 (180)	0.20 (350)
H-Y-6	709	184	526	0.26	0.22	0.48	3.3	0.32 (178)	0.39 (318)
H-Y-30	814	259	556	0.27	0.29	0.56	2.9	0.09 (169)	0.25 (329)
H-Y-40	658	243	416	0.20	0.29	0.49	3.1	0.06 (154)	0.15 (309)
reused H-Y-30[c]	830	260	570	0.28	0.28	0.56	2.9	0.10 (159)	0.24 (334)
Pd/H-Y-30	781	249	533	0.26	0.29	0.55	3.0	0.12 (162)	0.23 (320)
Pd/H-Y-40	620	199	421	0.21	0.25	0.46	3.3	0.08 (159)[d]	0.24 (293)[d]

[a] Adsorption–desorption isotherms, PSD curves, and TPD-NH_3 profiles are presented in the Supporting Information. [b] Parent zeolite (calcined NH_4-Y, Si/Al ratio of 2.55, CBV300). [c] After third reuse and (re)calcination. [d] Estimated values from poorly resolved desorption peaks (Figure S12).

NH_4-Y-2.55, whereas H-Y-30 and H-Y-40 are obtained after an extra steaming step and acid-leaching step from NH_4-Y-2.55.[10c,12] The textural properties of the different H-Y-*x* zeolite materials under study are summarized in Table 1. As expected, N_2 physisorption measurements showed that the ultrastabilization of zeolite H-Y resulted in an increase in the BET surface area (providing a value proportional to the volume adsorbed for these microporous systems), *t*-plot external surface area, and total pore volume. The presence of mesopores in zeolite H-Y-2.6 is likely the result of the partial dealumination of the zeolite framework. The further increase in mesopore volume upon increasing the Si/Al ratio is in line with previous reports.[9,10] As expected, H-Y-40 gave the highest $V_{mesopore}/V_{total}$ ratio of 59%, followed by H-Y-30 (52%, the same $V_{mesopore}$), H-Y-6 (46%), and H-Y-2.6 (41%). Hysteresis loops were observed in the adsorption and desorption isotherms for the various H-Y zeolites (Figure S1), typical of such mesoporous materials.[9] The pore size distribution (PSD) curves from the desorption branch exhibit a sharp peak at ~4 nm and a peak that broadens as the extent of dealumination increases (e.g., ~4–20 and ~4–45 nm for H-Y-2.6 and H-Y-30, respectively; Figure S2), which supports the increase in the degree of mesoporosity. Furthermore, the peak maxima show a gradual shift to larger pore diameters with the increase of the Si/Al ratio, which is a consequence of the increasing amount of EFAl species removed by the acid treatment.[9]

The total amount of acid sites in H-Y zeolites, as measured by temperature-programmed desorption of ammonia (TPD-NH_3), decreased in the order H-Y-6 > H-Y-2.6 > H-Y-30 > H-Y-40 (Table 1). Both H-Y-6 and H-Y-2.6 contain large amounts of weak acid sites (i.e., Lewis acid sites, LAS), whereas H-Y-30 and H-Y-40 do not (Figure S3). For both types of acid sites, a shift of the desorption maximum (T_{max}) towards a lower temperature is observed as the extent of dealumination increases, except for H-Y-30. In terms of the amount and strength of acid sites, H-Y-40 is the least acidic and is expected to contain the lowest quantity of EFAl species.

Fourier-transform infrared (FTIR) spectra of the four H-Y zeolites and the parent sample under dehydrating conditions (300 °C, 10^{-5} mbar) show three distinct peak maxima located at $\tilde{\nu} \approx 3748$ (Si–OH silanol groups), 3640 (OH groups in supercages), and 3555 cm^{-1} (OH groups in small cavities) observed for H-Y-6, H-Y-30, and H-Y-40 (Figure S4), which correspond to strong framework OH groups (BAS).[13] Three additional peaks at $\tilde{\nu} \approx 3660$ (Al–OH groups),[13b] 3600 (strong),[13c] and 3518 cm^{-1} (shoulder) were seen only in steamed and partially acid-leached H-Y-6, which can explain the high amount of acid sites of this sample. The stepwise adsorption of CO on the five H-Y zeolites at low temperature provided additional insights into the type, strength, and distribution of their acid sites (Figure S5–S9). The distinct *v*(OH) band at $\tilde{\nu} \approx 3640$ cm^{-1} is perturbed first at low equilibrium CO pressures and gives rise to the development of a *v*(OH) band at $\tilde{\nu} \approx 3275$ cm^{-1} accompanied by two broad bands near $\tilde{\nu} \approx 3410$ and 3465 cm^{-1}, in agreement with previous reports.[13] Simultaneously, the *v*(CO) stretching band at $\tilde{\nu} \approx 2180$ cm^{-1} grows (LAS). The low-frequency OH stretching band at $\tilde{\nu} \approx 3555$ cm^{-1} was not perturbed by CO because CO cannot access the small sodalite cages.[13]

As shown previously, EFAl species contribute significantly to the generation of both the LAS and BAS of H-Y zeolites.[13] The acidity of their OH groups is evident in the pronounced *v*(CO) band in H-Y-2.6 and H-Y-6 centered at $\tilde{\nu} \approx 2165$ cm^{-1} at relatively low equilibrium CO pressures, for example, ~0.6 mbar (Figure 1a). Notably, the appearance of the well-known band at $\tilde{\nu} = 2158$ cm^{-1}, recorded for H-Y-30 and H-Y-40 only, is attributed to the interaction of SiOH with CO.[13e] The appearance of a (weak) shoulder at $\tilde{\nu} \approx 3465$ cm^{-1} (in H-Y-6) accompanied by another one at $\tilde{\nu} \approx 3530$ cm^{-1} (in H-Y-2.6 and H-Y-6) after CO adsorption at, for example, ~1 mbar (Figure 1b), further demonstrates the presence of such acidic EFAl species, as observed previously.[13a]

Two bifunctional catalysts, 1 wt% Pd/H-Y-30 and 1 wt% Pd/H-Y-40, were synthesized by incipient wetness impregnation. The $V_{mesopore}$ of Pd/H-Y-30 is the same as that of H-Y-30, but the micropore area and volume decreased, which suggests that some of the Pd nanoparticles (3.1 ± 0.7 nm, determined by transmission electron microscopy, TEM; Figure S10) are possibly located in the microporous domains.[14] The CO-FTIR spectra of Pd/H-Y-30 revealed the effect of Pd incorporation on the

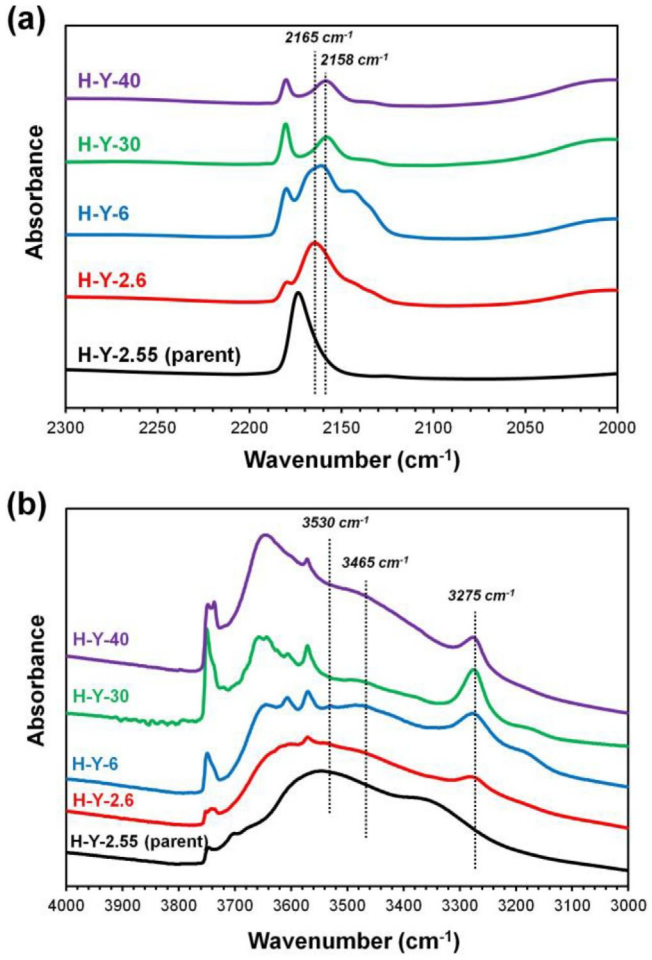

Figure 1. Low-temperature FTIR spectra of the dehydrated H-Y-*x* zeolites (*x* = Si/Al ratio) in the a) *v*(CO) region at ~0.6 mbar CO and b) *v*(OH) region at ~1 mbar CO. Stepwise, low-temperature CO-FTIR spectra of the five zeolite H-Y materials under study are presented in Figures S5–S9.

acidity of the framework OH groups, as evidenced in the reduced intensity of the bands of both silanols and bridging Si(OH)Al groups compared to the parent H-Y-30 sample (Figure S11). The reduction in the number of strong acid sites (BAS) was in agreement with the reduced amount and strength of the high-temperature NH_3 desorption peak of Pd/H-Y-30 (Table 1, Figure S12). In Pd/H-Y-40, a decrease in the mesopore volume and a clear shift of the peak maximum in the PSD curve (Figure S14b) suggest that a significant portion of the Pd nanoparticles (5.1 ± 1.4 nm; Figure S13) are located in the mesopore domains. Indeed, the *v*(OH) intensity of the strong acid sites of H-Y-40 and Pd/H-Y-40 are very similar with or without CO (Figure S15). For both bifunctional catalysts, the observed increase in the amount of desorbed NH_3 at low temperature can be attributed to various amounts of Lewis acidic Pd centers.[14b]

Catalyst testing: Zeolites

The one-pot catalytic aromatization of the hydrogenated DA adduct of 2-methylfuran and maleic anhydride (MFMA[H] **1**) to 3-methylphthalic anhydride **4** using H-Y-2.6 in combination with Pd/C is presented in Scheme 1. The γ-lactone **2** (primary intermediate) and the *m*-/*o*-toluic acids **5a**/**b** are also included. As aromatization and decarboxylation were also shown previously to occur to a limited extent in the presence of only H-Y-2.6,[7] the catalytic aromatization of **1** was first investigated with the acidic zeolites listed in Table 1 under reaction conditions established previously (1.0 g of **1**, 200 °C, 24 h in toluene).[7]

Among the four H-Y zeolites under study (10 wt% relative to **1**), H-Y-2.6 is the least active, but nevertheless shows high selectivity to the desired product **4** (Table 2, entries 1–4). Notably, the use of only the H-Y zeolites allowed the observation and identification of an additional intermediate, the 1,3-diene anhydride isomer **3**, which is suggested to be formed by zeolite-catalyzed lactone ring opening followed by anhydride formation. The identification of this intermediate was based on the typical ^{1}H NMR spectroscopic signature of the conjugated 1,3-cyclohexadiene ring (Figure S16). Moreover, the liquid-phase zeolite-only-catalyzed aromatization reactions are accompanied by the formation of small amounts of the transfer

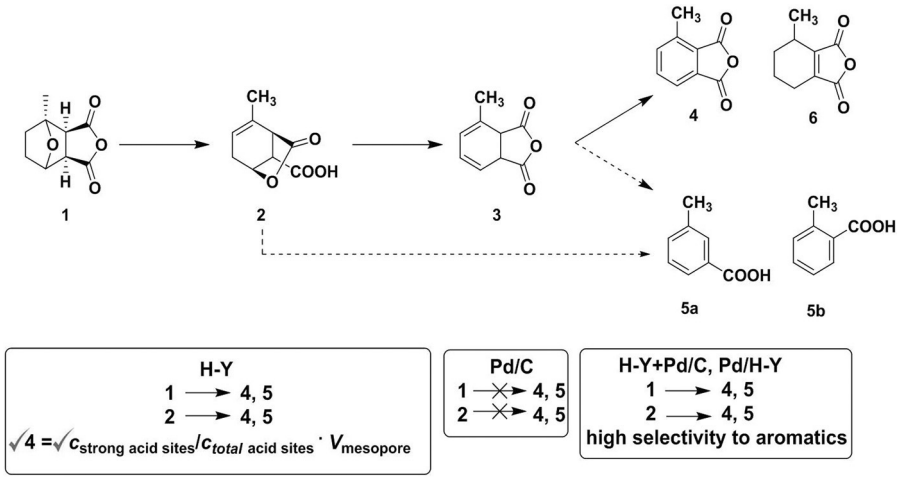

Scheme 1. Final step of the three-step (DA addition, hydrogenation, and catalytic aromatization) strategy to produce furan-derived aromatic compounds **4** and **5** using (tandem) zeolite H-Y and Pd/C and bifunctional Pd/H-Y catalysts.

Table 2. Reactivity of **1** with various zeolite H-Y catalysts.[a]

Entry	Solid catalyst(s)	Catalyst loading[b]	Conversion[c] [mol%]	Yield [mol%] (selectivity [mol%])[c] 2	3	4	5a	5b	6	Total aromatics yield (selectivity)[d] [%]	Mole balance[e] [%]
1	H-Y-2.6	10	58	21 (36)	8 (14)	12 (21)	4 (7)	–[f]	1 (2)	16 (28)	88
2	H-Y-6	10	74	44 (59)	8 (11)	10 (14)	4 (5)	2 (3)	1 (2)	16 (22)	95
3	H-Y-30	10	96	47 (49)	14 (15)	17 (18)	6 (6)	3 (3)	2 (2)	26 (27)	93
4	H-Y-40	10	91	45 (49)	19 (21)	14 (15)	3 (3)	–[f]	3 (3)	17 (18)	93
5	H-Y-40 + Pd/C	10 + Pd/C[g]	94	31 (33)	–[f]	45 (48)	9 (10)	2 (2)	1 (1)	56 (60)	94
6	H-Y-2.6	33	100	14	2	25	21	14	7	60	83
7	H-Y-6	33	100	–[f]	9	33	24	14	6	71	86
8	H-Y-30	33	100	–[f]	17	44	15	8	7	68	91
9	H-Y-40	33	100	–[f]	12	40	18	11	9	69	90

[a] Conditions: 1.0 g **1**, 200 °C, 24 h in toluene, Ar atmosphere (1 bar), catalyst(s) is indicated in the table. [b] wt% relative to **1**. [c] Calculated by using q-NMR spectroscopy using dimethyl 3,4-furan dicarboxylate as internal standard. [d] **4+5a+5b**. [e] Mole balance determined from the total number of moles calculated from the crude mixture after the reaction by NMR analysis. [f] Not observed. [g] 1 wt% Pd relative to H-Y-40.

hydrogenation product (4-methyl-4,5,6,7-tetrahydroisobenzofuran-1,3-dione **6**), thought to result from (an isomer of) **3** by double bond isomerization/hydrogenation as well as by the release of H_2 (Table S1). Trace metal analysis of the H-Y samples showed negligible concentrations of potential metal impurities (Table S2) that could catalyze the required dehydrogenation step; the acceptor-less H_2 evolution step is, therefore, suspected to be noncatalytic under these reaction conditions. H-Y-30 is the most active catalyst, as 96% of **1** is converted and it gives the highest total aromatics yield. Clearly, the conversion order does not depend on the total acidity but more importantly on a combination of the nature of the acid sites and mesoporosity and external surface area, as illustrated below. The γ-lactone **2** is the major product with all four zeolites, and its accumulation at higher conversions suggests that it is involved in the rate-determining step of the reaction. Both the conversions and yields to **2** shown by H-Y-30 and H-Y-40 are comparable (Table 2, entries 3 and 4), which demonstrates a similar performance toward the acid-catalyzed isomerization of **1**. However, their total aromatics yields differ markedly, which suggests that the number and type of acid sites matter at the same mesoporosity (vide infra). The selectivity ratio of **4** to total aromatics (*S***4**/*S***4**+*S***5a+b**) using H-Y-40 is significantly higher at 83% than with H-Y-30 (67%), noting that the former catalyst showed slightly lower activity and limited yields of **5a**/**b**.

The γ-lactone **2** was then synthesized, isolated, and used as a substrate for aromatization reactions with H-Y-30 and H-Y-40 (10 wt% relative to **2**) under the same conditions (Table 3, entries 1 and 2). These reactions resulted in the formation of the same aromatic products, which emphasizes the role of **2** as a primary intermediate, with H-Y-30 again slightly more active and selective to **4** than H-Y-40. Notably, however, the yields of aromatic products are significantly higher than those observed if **1** was used as the substrate, indicating a change in acidity requirement for further conversion of **2** compared to the conversion of **1** to **2**. The formation of decarboxylation products was especially favored if we started from intermediate **2**, as indicated by an increase in the selectivity ratios of **5a**/**b** to total aromatics for zeolites H-Y-30 (from 33 to 48%) and H-Y-40 (from 17 to 51%), which suggests that the formation of aromatic products **4** and **5a**/**b** have different orders in **2** and involve different reaction pathways (i.e., **5a/b** are not obtained from **4** in the zeolite-only reactions).

The increase of the amount of different H-Y zeolites from 10 to 33 wt% (relative to **1**) resulted in the full conversion of **1** for all catalysts, and intermediate **2** was not detected anymore for H-Y-6, H-Y-30, and H-Y-40 (Table 2, entries 6–9). H-Y-30 again gave the highest amount of **4**, which showed a more than two-fold increase in yield. H-Y-6, which is the most acidic zeolite (Table 1) but was treated much more moderately than H-Y-30, gave the highest total aromatics yield at 71% at this higher catalyst loading. However, H-Y-6 and H-Y-2.6 showed considerably lower yields of **4** and noticeably higher yields of **5a+b**. Indeed, the low-Si/Al-ratio H-Y zeolites show a higher selectivity for decarboxylation (red and green bars, Figure 2),

Table 3. Reactivity of **2** with H-Y-30 and H-Y-40 with or without a Pd/C catalyst.[a]

Entry	Solid acid catalyst	Catalyst loading[b]	Pd/C loading[c]	Conversion [mol%]	Yield [mol%] (Selectivity [mol%])[d] 3	4	5a	5b	6	Total aromatics yield (selectivity)[e] [%]	Mole balance[f] [%]
1	H-Y-30	10	0	93	11 (12)	30 (32)	21 (23)	6 (6)	6 (6)	57 (61)	81
2	H-Y-40	10	0	90	14 (16)	27 (30)	20 (22)	8 (9)	7 (8)	55 (61)	86
3	H-Y-40	10	1	94	–[g]	50 (53)	28 (30)	4 (4)	5 (5)	82 (87)	93

[a] Conditions: 1.0 g **2**, 24 h in toluene, 200 °C, Ar atmosphere (1 bar), catalyst(s) indicated in the table. [b] wt% relative to substrate **2**. [c] wt% Pd relative to H-Y-40. [d] Calculated by using q-NMR spectroscopy using dimethyl 3,4-furan dicarboxylate as internal standard. [e] **4+5a+5b**. [f] Mole balance determined from the total number of moles calculated from the crude mixture after the reaction by NMR analysis. [g] Not observed.

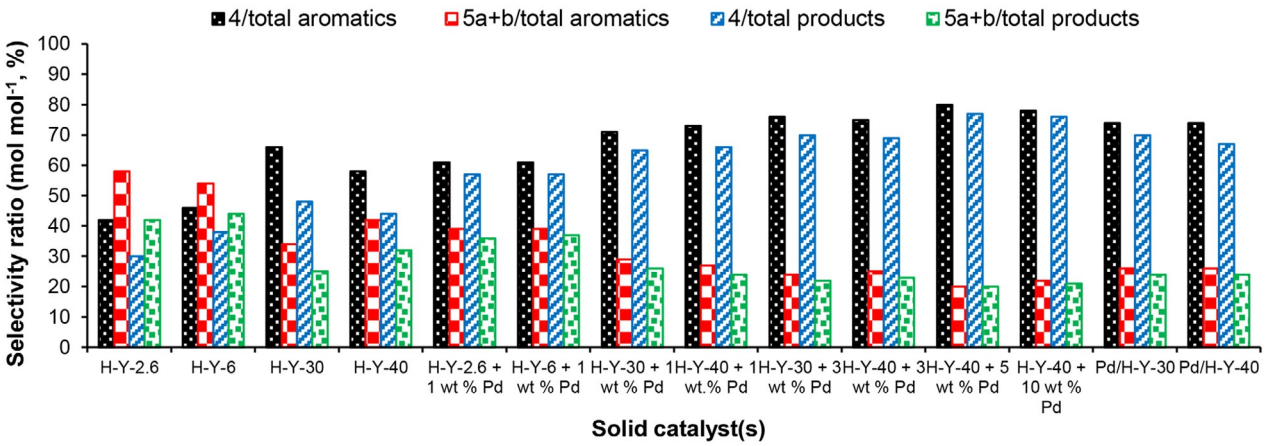

Figure 2. Selectivity ratios of aromatic products from **1** using solid acid catalysts (33 wt% relative to **1**) with and without Pd. Results calculated from the data presented in Tables 2, 4, and 5.

whereas H-Y-30 and H-Y-40 are in turn (much) more selective for the production of **4** (black and blue bars). These results may indicate that weak acid sites are involved in the decarboxylation reaction. That H-Y-2.6 and H-Y-6 also contain strong acid sites yet their selectivity to **4** is relatively low suggests that their much higher concentration of weak acid sites than in H-Y-30 and H-Y-40 pushes the reaction more towards decarboxylation. However, as shown above, the mesoporosity of zeolites also changed on going from H-Y-2.6 to H-Y-6 and H-Y-6 to H-Y-30. Thus, the high selectivity of H-Y-30 to **4** must also reflect the positive effects of enhanced mesoporosity and external surface area because of the effective removal of agglomerated extra-framework materials that could hinder access to the active sites. These effects seem to affect the selectivity to **4** more strongly than the amount of strong acid sites and a higher strong-to-weak acid site ratio in H-Y-6. Importantly, on going from H-Y-30 to H-Y-40, the $V_{mesopore}$ remained constant, which allowed the influence of the acid type ratio to be assessed. With a strong acid sites and strong-to-weak acid site ratio that is lower for H-Y-40, a decrease in the selectivity to **4** (Table 2, entries 8 and 9) is then in line with the above. Taken together, zeolite-only-catalyzed aromatization reactions clearly show the need for a balanced concentration of acid sites and accessibility to these sites to attain high selectivity to the desired aromatic product. A strong correlation is thus found to exist between the yield of 3-methylphthalic anhydride **4** at full conversion and an acidity–mesoporosity coefficient, a combined metric defined as the product of $c_{strong\ acid\ sites}/c_{total\ acid\ sites}$ and $V_{mesopore}$ of the H-Y zeolites (Figure 3). Recently, Keller et al. introduced this performance descriptor for a zeolite-catalyzed condensation reaction to emphasize the importance of the combined influence of acidity and accessibility.[10d] A similar correlation is observed if the selectivity ratio of **4** to total aromatics is plotted against the same acidity–mesoporosity coefficient (Figure 3).

The reusability of H-Y-30, the best-performing solid acid catalyst, was also assessed. H-Y-30 can be recycled efficiently after regeneration by washing and calcination and gives the same distribution of aromatic products after each reuse and regener-

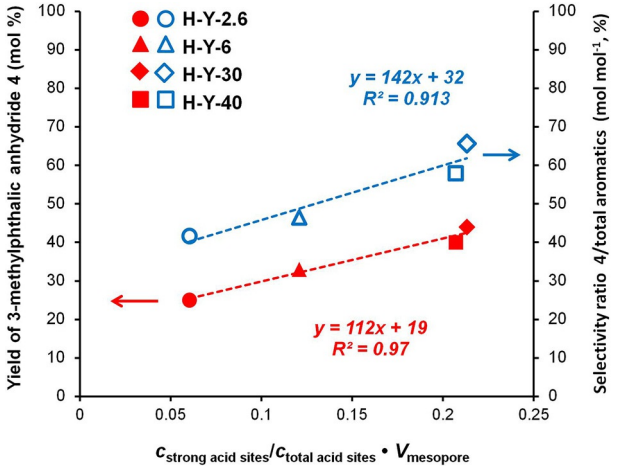

Figure 3. Correlation between the yield of **4** (full symbols) and selectivity ratio of **4** to total aromatics (*S***4**/*S***4**+*S***5a**+*S***5b**; open symbols), and the acidity–mesoporosity coefficient ($c_{strong\ acid\ sites}/c_{total\ acid\ sites}{\cdot}V_{mesopore}$)[10d] of the four H-Y catalysts at the full conversion of **1** (33 wt% H-Y relative to **1**). Results calculated from data presented in Tables 1 and 2.

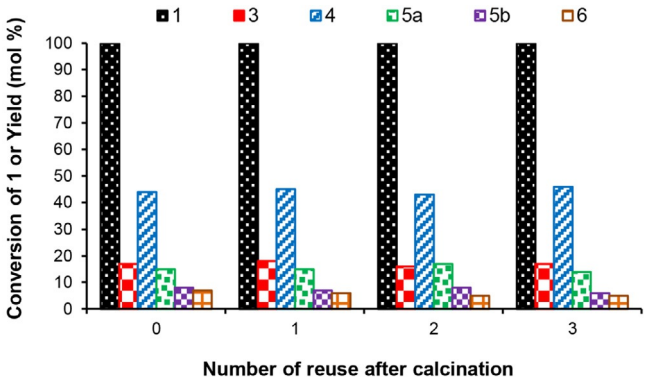

Figure 4. Recyclability of H-Y-30 in the aromatization of **1** (1.0 g of **1**, 33 wt% H-Y relative to **1**, 200 °C, 24 h in toluene, Ar atmosphere (1 bar); regeneration by washing and calcination at 500 °C, 6 h).

ation (Figure 4). Indeed, TPD-NH_3 experiments show that the total amount of acid sites remained the same after the third reuse and (re)calcination (Table 1 and Figure S17). Furthermore, the textural properties of the reused zeolite catalyst did not change significantly, in line with its stable catalytic performance.

Catalyst testing: Zeolites combined with Pd/C

It was shown previously that an increase in temperature from 150 to 200 °C using H-Y-2.6 (10 wt% relative to **1**) was necessary to increase the conversion of **1** and the selectivity to the desired aromatic product **4**.[7] At 200 °C, the addition of Pd/C as a dehydrogenation catalyst (3 wt% relative to **1**) to H-Y-2.6 (10 wt% relative to **1**) was also shown to increase the yield of **4** from 22 to 56% and, consequently, the total aromatics yield from 26 to 75%.[7] Here we show that for various H-Y zeolites in the presence of Pd/C, the increase in temperature from 150 (Table S3) to 200 °C (Table 2) indeed resulted in a significant increase in yield and selectivity to aromatic products accompanied by a concomitant decrease in the yields of **2** and **3**. We varied the ratio of the solid acid to the dehydrogenation catalyst at 200 °C and furthermore found that already the addition of a very small amount of Pd/C even to the least acidic catalyst (i.e., H-Y-40) at low loading (10 wt% relative to **1**) dramatically increased the selectivity to **4** from 15 to 48%, primarily at the expense of **2** and **3** (Table 2, entries 4 and 5; Figure S18). The addition of Pd/C thus facilitates not only the dehydrogenation of diene intermediate **3** as expected, but it also influences the further conversion of the γ-lactone intermediate **2**. The latter is remarkable as Pd is not directly involved in the first step after **2**, as evidenced by the reaction of γ-lactone **2** and Pd/C, which gives no conversion. Similarly, the conversion of **1** is not affected by the addition of the Pd/C catalyst as the first step is purely acid catalyzed and the Pd/C adds very little to the overall acidity of the system. Furthermore, the selectivity ratio of **4** (80 vs. 83%) and **5a+b** (17 vs. 20%) to total aromatics only changed slightly in H-Y-40 with or without Pd (Figure 2), which illustrates that the selectivity is dominated by zeolite-catalyzed steps and can thus be controlled by the modification of this catalyst only at this catalyst ratio. A comparison of the reaction of intermediate **2** with 10 wt% of H-Y-40 with or without Pd/C shows that the addition of the dehydrogenation catalyst gives a higher selectivity to **4** with Pd/C present (Table 3, entries 2 and 3; Figure S19), which suggests that the dehydrogenation catalyst pulls the reaction to **4** rather than to decarboxylation (i.e., the yield of **4** increases much more than the yield of **5a+5b**). Indeed, as Pd is known for both dehydrogenation as well as decarboxylation activity,[15] these results suggest that the former type of reactivity dominates under the applied conditions. This effect is even more pronounced if the reaction of **1** and intermediate **2** with the combination of Pd/C and H-Y-40 are compared. The results thus show that even though Pd/C is not involved directly in the conversion of **1** to **2**, nor in the first step that **2** subsequently undergoes, the Pd/C catalyst can influence the equilibria involved in such a way that is beneficial for both total aromatics yield and the selectivity to the desired aromatic product **4**. This could, for example, be the result of the (rapid isomerization and) dehydrogenation of the diene intermediate to give the aromatic anhydride product **4**. The latter was shown previously to be stable under reaction conditions,[7] which suggests that the alternative decarboxylation pathway should precede aromatization and involves the 1,3-diene anhydride or its diacid precursor.[16] Pd/C addition then effectively suppresses this pathway if present in sufficient amounts.

An increase of the catalyst loading for the zeolite-only reactions had a positive influence in terms of aromatic product yield and selectivity (Table 2). The catalytic performance of the four H-Y zeolite catalysts with 1 wt% Pd/C was, therefore, tested at 33 wt% loading. The full conversion of **1** is now attained, and **2** and **3** are not observed anymore for any combination of catalysts (Table 4). Similar total aromatics yields are obtained for the four H-Y catalysts, but selectivities differ considerably. Indeed, the high-Si/Al-ratio H-Y-30 and H-Y-40 again show the highest selectivities to **4**, whereas H-Y-2.6 and H-Y-6 produced more of the toluic acids, which is also seen with the zeolite-only runs (Table 2). If H-Y-40 is used, for example, the selectivity to **5a+b** is only 21%, which is escalated to 32 and 34% if H-Y-2.6 and H-Y-6 are used, respectively (Table 4, entries 1, 2, and 5). Comparing these results to the 33 wt% zeolite-only results and to the 10 wt% H-Y with/without 1 wt%

Table 4. Reactivity of **1**[a] with various H-Y zeolites with added Pd/C catalyst.[b]

Entry	Solid acid catalyst	Pd/C loading[c]	Yield/selectivity [mol%][d] **4**	**5a**	**5b**	**6**	Total aromatics yield (selectivity)[e] [%]	Mole balance[f] [%]
1	H-Y-2.6	1	51	27	5	6	83	89
2	H-Y-6	1	53	29	5	6	87	93
3	H-Y-30	1	59	19	5	8	83	91
4	H-Y-30	3	64	17	3	7	84	91
5	H-Y-40	1	57	17	4	10	78	88
6	H-Y-40	3	61	16	4	7	81	88
7	H-Y-40	5	71	14	4	3	89	92
8	H-Y-40	10	68	15	4	3	87	90

[a] Full conversion of substrate **1**; intermediates **2** and **3** were not detected. [b] Conditions: 1.0 g of **1**, 24 h in toluene, 200 °C, Ar atmosphere (1 bar), 33 wt% H-Y relative to **1**. [c] wt% Pd relative to H-Y. [d] Calculated by using q-NMR spectroscopy using dimethyl 3,4-furan dicarboxylate as internal standard; Yield = Selectivity. [e] **4+5a+5b**; Yield = Selectivity. [f] Mole balance determined from the total number of moles calculated from the crude mixture after the reaction by NMR spectroscopy.

Pd/C results shows that at the higher zeolite loadings, the amount of Pd added is not sufficient to drive the reaction towards the desired product and achieve the same gain in selectivity seen for the 10 wt% zeolite reactions with Pd. Indeed, as the zeolite dominates the conversion, the aromatic product selectivity in the reactions with Pd at higher zeolite loadings becomes more similar to that of the zeolite-only reactions.

As expected, the selectivity to the desired aromatic product **4** can then be further improved by increasing the amount of dehydrogenation catalyst, as shown for H-Y-30 and H-Y-40 (Table 4 and Figure 2). For example, the selectivity of H-Y-30 to **4** and **5a+b** changed from 59 and 24 to 64 and 20% at 1 and 3 wt% Pd, respectively, (Table 4, entries 3 and 4; Figure S20). The same enhancement was observed for H-Y-40, for which an increase of the Pd loading to 5 wt% resulted in increased yields of **4**, a (slight) decrease in decarboxylation, and a decrease in the transfer hydrogenation product **6**. A further increase of Pd/C to 10 wt% at constant zeolite H-Y-40 loading, however, did not result in any significant improvement in selectivity and aromatic product distribution, which suggests that the optimum amount of Pd is 5–10 wt% to give 71% as the highest selectivity to **4**. Pd/C alone at 10 wt% without H-Y showed no conversion of **1**.

Catalytic testing: Bifunctional Pd/H-Y catalysts

The results above show that the combination of Pd/C with H-Y-30 or H-Y-40 is preferred in terms of selectivity to **4** and are hence used as basis to prepare the bifunctional catalysts 1 wt% Pd/H-Y-30 and 1 wt% Pd/H-Y-40. At 33 wt% loading, Pd/H-Y-30 and Pd/H-Y-40 catalysts give *S***4**/*S* total products ratios of 70 and 67%, respectively, at a full conversion of **1**, which is higher than the corresponding physical mixtures (Figure 2). The bifunctional catalysts were also tested for other substrate combinations (Table 5, entries 3–6). Using furan as the diene in the aromatization reaction, lower activity and selectivity for phthalic anhydride were obtained than for **1** as substrate for both catalysts. In contrast, significantly higher yields of total aromatics of up to 90% could be obtained with the 2,5-dimethylfuran-derived hydrogenated DA adduct using the bifunctional catalysts 1 wt% Pd/H-Y. At full conversion, the selectivity ratio of 3,6-dimethylphthalic anhydride to total aromatics (3,6-dimethylphthalic anhydride+*p*-xylene+2,5-dimethylbenzoic) is 78%, compared to 74% for **1**. These differences in the reactivity of the three different hydrogenated DA adducts coincide with the ease of the acid-catalyzed ring opening of the oxanorbornane ring, which depends on the furan substitution pattern.[7] *p*-Xylene was detected with the 2,5-dimethylfuran-derived hydrogenated DA adduct in yields up to 21%.

Conclusions

We have demonstrated that hierarchically structured FAU-type zeolites are highly efficient solid acid catalysts in the liquid-phase conversion of furanics-derived hydrogenated Diels–Alder adducts to renewable aromatic chemicals. Key to their catalytic performance is the enhanced mesoporosity and external surface area upon dealumination balanced with (accessible) Brønsted acid concentration. The addition of a dehydrogenation catalyst, that is, Pd/C, improves the selectivity to aromatic products significantly at the expense of the γ-lactone and the newly identified 1,3-diene intermediates. Furthermore, the addition of Pd/C improves the selectivity of aromatic anhydride formation strongly over toluic acid formation. The dependence of selectivity on Pd concentration strongly suggests that efficient coupling of the steps is essential to drive the reaction towards the formation of the desired aromatic product 3-methyphthalic anhydride. By optimizing the Pd-to-H-Y zeolite ratio, the competitive decarboxylation reaction can thus be effectively suppressed. The aromatic product selectivity can also now be tuned by controlling the vicinity of the dehydration and dehydrogenation functionalities and, more importantly, by careful choice of the zeolite H-Y catalyst used. The synthesized bifunctional Pd/H-Y catalysts were also highly selective for the aromatization of other hydrogenated Diels–Alder furan derivatives. Overall, the zeolite component dominates the catalyst selectivity, and the acidity–mesoporosity coefficient is again

Table 5. Reactivity of different hydrogenated DA adducts using bifunctional Pd/H-Y catalysts.[a]

Entry	Solid catalyst[b]	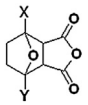	Conversion[c] [mol%]	Yield [mol%] (Selectivity [mol%])[c] 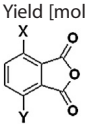	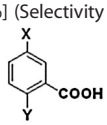	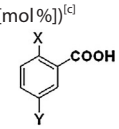	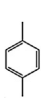	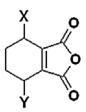	Total aromatics yield (selectivity)[d] [%]	Mole balance[e] [%]
1	Pd/H-Y-30	X = CH_3, Y = H	100	64	18	4	–[f]	6	86	92
2	Pd/H-Y-40	X = CH_3, Y = H	100	60	18	3	–[f]	8	81	89
3	Pd/H-Y-30	X = Y = H	85	41 (48)	25 (29)[g]		–[f]	9 (11)	66 (77)	90
4	Pd/H-Y-40	X = Y = H	82	45 (55)	16 (20)[g]		–[f]	12 (15)	61 (75)	91
5	Pd/H-Y-30	X = Y = CH_3	100	62	7[h]		21	–[i]	90	90
6	Pd/H-Y-40	X = Y = CH_3	100	69	4[h]		16	–[i]	89	89

[a] Conditions: 1.0 g of substrate, 24 h in toluene, 200 °C, Ar atmosphere (1 bar), 33 wt% Pd/H-Y relative to substrate. [b] Contained 1 wt% Pd relative to H-Y. [c] Calculated by using q-NMR spectroscopy using dimethyl 3,4-furan dicarboxylate as internal standard. [d] **4+5a+5b**; phthalic anhydride+benzoic acid; 3,6-dimethylphthalic anhydride+*p*-xylene+2,5-dimethylbenzoic acid. [e] Mole balance determined from the total number of moles calculated from the crude mixture after the reaction by NMR spectroscopy. [f] Not applicable. [g] Benzoic acid. [h] 2,5-Dimethylbenzoic acid. [i] Not observed.

shown to be a key structure–performance indicator, in this case for tandem catalytic aromatization. Ongoing computational studies are expected to provide further detailed insights into the mechanistic pathways to the observed aromatics, in particular the decarboxylation products.

Experimental Section

Preparation of substrates and catalysts

The materials and methods used for the synthesis of (hydrogenated) DA adducts and γ-lactone intermediate **2** were reported previously.[7] All zeolite Y catalysts used in this study were obtained from Zeolyst International (CBV300, NH_4-Y, Si/Al = 2.55; CBV600, H-Y, Si/Al = 2.6; CBV712, NH_4-VUSY, Si/Al = 6; CBV760, H-SDUSY, Si/Al = 30; and CBV780, H-SDUSY, Si/Al = 40) and pretreated by heating them in stagnant air at 550 °C (10 °C min^{-1}) for 6 h. Pd/C (10 wt% Pd on activated carbon) was obtained from Sigma–Aldrich and used as received. Tetraamminepalladium(II) nitrate (10 wt% in water, Sigma–Aldrich) was used as the precursor for the synthesis of bifunctional Pd/H-Y catalysts. The bifunctional catalysts Pd/H-Y-30 and Pd/H-Y-40 (1 wt% Pd relative to H-Y) were prepared by incipient wetness impregnation. After the overnight evaporation of water at RT, the solids were further dried overnight at 60 °C and then overnight at 120 °C. The solids were ground, heated at 400 °C (5 °C min^{-1}) for 6 h under N_2 flow (100 mL min^{-1}), and finally reduced by heating from RT to 200 °C (5 °C min^{-1}) for 6 h under flowing pure H_2 (60 mL min^{-1}).

Catalyst characterization

The textural properties of the zeolite materials were determined by using a Micromeritics Tristar 3000 set-up. The N_2 physisorption experiments were conducted at 77 K after initial pretreatment of the samples by degassing at 300 or 400 °C for 12 h in a N_2 flow. The apparent surface area was determined using the BET method. The total pore volume was determined from the single-point adsorption isotherm, and the micropore volume was determined from the *t*-plot analysis. The pore size and PSD were derived from the desorption isotherm according to the Barrett–Joyner–Halenda (BJH) method. The overall acidity of the catalysts was determined by TPD-NH_3 by using a Micromeritics ASAP 2920 instrument. Typically, the sample (100 mg) in a quartz reactor was dried in a He flow by heating (5 °C min^{-1}) from RT to 600 °C. Subsequently, the sample was cooled to 100 °C and NH_3 pulses (10 vol% in Ar) were applied at this temperature to eliminate physically adsorbed NH_3. The sample was then heated to 600 °C at 5 °C min^{-1} to induce desorption under flowing He. The desorbed NH_3 was quantified by using a thermal conductivity detector (TCD), obtained by integrating two clearly distinguishable peaks to determine the distribution of weak (low temperature range) and strong (high temperature range) acid sites. The total amount of NH_3 desorbed was taken as the total amount of acid sites. The FTIR spectra of the solid acids were recorded by using a PerkinElmer 2000 spectrometer (32 scans, 1000–4000 cm^{-1}) using CO as a probe for acidic sites. Typically, a self-supporting catalyst wafer (~0.017 g) was positioned inside a synchrotron cell equipped with a CaF_2 window. The cell was evacuated to high vacuum (~10^{-5} mbar), and the sample was dried in situ at 300 °C (5 °C min^{-1}) for 1 h. The cell was then cooled to −189 °C with liquid N_2 and connected to a gas chamber equipped with a pressure gauge that permitted the addition of an accurately known CO (10 vol% in He) pressure into the cell. Morphological studies were performed by using a Zeiss DSM982 Gemini field-emission scanning electron microscope with a Schottky emitter operated at 2.0 kV. TEM measurements were conducted in the bright-field imaging mode by using a Tecnai 20FEG transmission electron microscope operated at 200 kV. The mean particle size of Pd in the bifunctional catalysts was calculated from at least 117 different particles observed by using TEM. Trace metals in H-Y zeolites were quantified by using inductively coupled plasma atomic emission spectroscopy (ICP-AES, Spectro Acros) after dissolution in aqua regia.

Catalytic testing and spent catalyst regeneration

The catalytic reaction was performed in a continuously stirred 50 mL Parr batch reactor. Typically, the reactor was charged with 1.0 g of hydrogenated DA adduct, catalyst(s), and 30 mL of toluene. The reactor was then flushed with Ar, and the temperature was increased to 150 or 200 °C and held for 24 h. The reactor was submerged in ice-cold water to quench the reaction rapidly. The catalyst was separated from the mixture by centrifugation and filtration and washed extensively with toluene. The solvent was evaporated under reduced pressure by using a rotary evaporator to obtain the crude product. The identification of **2**, **4**, **5a**, **5b**, and **6** from the ^1H NMR spectra of the crude products was based on the reported ^1H NMR spectra of the isolated and purified products as described and adopted previously.[7,8] The conversions and product yields were calculated from the ^1H NMR data using $CDCl_3$ and dimethyl 3,4-furandicarboxylate as solvent and internal standard, respectively. The H-Y zeolites were regenerated and reused by washing the spent catalysts with toluene and acetone, drying overnight at 60 °C, drying at 120 °C for 6 h, and finally heating to 500 °C (10 °C min^{-1}) for 6 h under flowing air until samples that were completely white were obtained. H_2 produced in the reaction was collected in a gasbag and quantified by using micro-GC (Varian CP490) equipped with a COX column and a TCD detector.

Acknowledgements

This work is part of the research program Technology Areas for Sustainable Chemistry (TASC), which is partly financed by the Netherlands Organization for Scientific Research (NWO).

Keywords: acidity · biomass · hydrogenation · palladium · zeolites

[1] a) P. J. Dauenhauer, G. W. Huber, *Green Chem.* **2014**, *16*, 382–383; b) P. C. A. Bruijnincx, B. M. Weckhuysen, *Angew. Chem. Int. Ed.* **2013**, *52*, 11980–11987; *Angew. Chem.* **2013**, *125*, 12198–12206.

[2] a) G. J. M. Gruter, F. Dautzenberg, (Avantium), EP1834950, **2007**; b) G. Wypych, *Handbook of Plasticizers, 1st ed.*, ChemTec Publishing and William Andrew Inc., Toronto-New York, **2004**; c) D. I. Collias, A. M. Harris, V. Nagpal, I. W. Cottrell, M. W. Schultheis, *Ind. Biotechnol.* **2014**, *10*, 91–105.

[3] a) C. L. Williams, C.-C. Chang, P. Do, N. Nikbin, S. Caratzoulas, D. G. Vlachos, R. F. Lobo, W. Fan, P. J. Dauenhauer, *ACS Catal.* **2012**, *2*, 935–939; b) C.-C. Chang, S. K. Green, C. L. Williams, P. J. Dauenhauer, W. Fan, *Green Chem.* **2014**, *16*, 585–588.

[4] D. Wang, C. M. Osmundsen, E. Taarning, J. A. Dumesic, *ChemCatChem* **2013**, *5*, 2044–2050.

[5] a) J. J. Pacheco, M. E. Davis, *Proc. Natl. Acad. Sci. USA* **2014**, *111*, 8363–8367; b) J. J. Pacheco, J. A. Labinger, A. L. Sessions, M. E. Davis, *ACS Catal.* **2015**, *5*, 5904–5913; c) M. Orazov, M. E. Davis, *Chem. Sci.* **2016**, *7*, 2264–2274.

[6] a) E. Mahmoud, D. A. Watson, R. F. Lobo, *Green Chem.* **2014**, *16*, 167 – 175; b) M. Shiramizu, F. D. Toste, *Chem. Eur. J.* **2011**, *17*, 12452 – 12457.
[7] S. Thiyagarajan, H. C. Genuino, M. Śliwa, J. C. van der Waal, E. de Jong, J. van Haveren, B. M. Weckhuysen, P. C. A. Bruijnincx, D. S. van Es, *ChemSusChem* **2015**, *8*, 3052 – 3056.
[8] S. Thiyagarajan, H. C. Genuino, J. C. van der Waal, E. de Jong, B. M. Weckhuysen, J. van Haveren, P. C. A. Bruijnincx, D. S. van Es, *Angew. Chem. Int. Ed.* **2016**, *55*, 1368 – 1371; *Angew. Chem.* **2016**, *128*, 1390 – 1393.
[9] J. Zečević, C. J. Gommes, F. Friedrich, P. E. de Jongh, K. P. de Jong, *Angew. Chem. Int. Ed.* **2012**, *51*, 4213 – 4217; *Angew. Chem.* **2012**, *124*, 4289 – 4293.
[10] a) A. H. Janssen, A. J. Koster, K. P. de Jong, *Angew. Chem. Int. Ed.* **2001**, *40*, 1102 – 1104; *Angew. Chem.* **2001**, *113*, 1136 – 1138; b) A. H. Janssen, A. J. Koster, K. P. de Jong, *J. Phys. Chem. B* **2002**, *106*, 11905 – 11909; c) D. Verboekend, N. Nuttens, R. Locus, J. Van Aelst, P. Verolme, J. C. Groen, J. Pérez-Ramirez, B. F. Sels, *Chem. Soc. Rev.* **2016**, *45*, 3331 – 3352; d) T. C. Keller, J. Arras, S. Wershofen, J. Pérez-Ramirez, *ACS Catal.* **2015**, *5*, 734 – 743; e) S. Mitchell, A. B. Pinar, J. Kenvin, P. Crivelli, J. Kärger, J. Pérez-Ramirez, *Nat. Commun.* **2015**, *6*, 8633.
[11] R. E. Patet, N. Nikbin, C. L. Williams, S. K. Green, C.-C. Chang, W. Fan, S. Caratzoulas, P. J. Dauenhauer, D. G. Vlachos, *ACS Catal.* **2015**, *5*, 2367 – 2375.
[12] a) J. Chen, Z.-C. Feng, P. Ying, C. Li, *J. Phys. Chem. B* **2004**, *108*, 12669 – 12676; b) Zeolyst International (website): http://www.zeolyst.com/our-products/standard-zeolite-powders/zeolite-y.aspx.
[13] a) O. Cairon, T. Chevreau, J.-C. Lavalley, *J. Chem. Soc. Faraday Trans.* **1998**, *94*, 3039 – 3047; b) A. Zecchina, S. Bordiga, G. Spoto, D. Scarano, G. Petrini, G. Leofanti, M. Padovan, C. Otero-Arean, *J. Chem. Soc. Faraday Trans.* **1992**, *88*, 2959 – 2969; c) S. Khabtou, T. Chevreau, J. Lavalley, *Microporous Mater.* **1994**, *3*, 133 – 148; d) S. M. Almutairi, B. Mezari, G. A. Filonenko, P. C. M. M. Magusin, M. S. Rigutto, E. A. Pidko, E. J. M. Hensen, *ChemCatChem* **2013**, *5*, 452 – 466; e) O. Cairon, *Phys. Chem. Chem. Phys.* **2010**, *12*, 6333 – 6336.
[14] a) J. Zečević, A. M. J. van der Eerden, F. Friedrich, P. E. de Jongh, K. P. de Jong, *ACS Nano* **2013**, *7*, 3698 – 3705; b) M. Jabłońska, A. Król, E. Kukulska-Zajac, K. Tarach, L. Chmielarz, K. Góra-Marek, *J. Catal.* **2014**, *316*, 36 – 46.
[15] a) R. W. Gosselink, S. A. W. Hollak, S.-W. Chang, J. van Haveren, K. P. de Jong, J. H. Bitter, D. S. van Es, *ChemSusChem* **2013**, *6*, 1576 – 1594; b) S. Matsubara, Y. Yokota, K. Oshima, *Org. Lett.* **2004**, *6*, 2071 – 2073; c) K. Nagayama, F. Kawataka, M. Sakamoto, I. Shimizu, A. Yamamoto, *Bull. Chem. Soc. Jpn.* **1999**, *72*, 573 – 580.
[16] M. R. DeCamp, B. J. Landon, *Tetrahedron Lett.* **1980**, *21*, 3231 – 3234.

Received: June 10, 2016
Revised: July 20, 2016
Published online on August 25, 2016

